Chemical Science

ROYAL SOCIETY OF CHEMISTRY

EDGE ARTICLE

View Article Online
View Journal | View Issue

Check for updates

Cite this: *Chem. Sci.*, 2026, **17**, 956

All publication charges for this article have been paid for by the Royal Society of Chemistry

Received 15th September 2025
Accepted 6th November 2025

DOI: 10.1039/d5sc07119d

rsc.li/chemical-science

Observation of thermally activated intersystem crossing in room-temperature phosphorescence of weakly donor–acceptor–donor π-ternary molecules

Wenbin Huang,[a] Chenlong Wei,[b] Yuxin Zhu,[b] Qian Zhang *[a] and Zikai He *[abc]

The direct observation of thermally activated intersystem crossing (TA-ISC) processes in room-temperature phosphorescence (RTP) has not been well investigated. Here, we reported four weakly donor–acceptor–donor π-ternary molecules featuring isomerism-dependent phosphorescence behaviors. The isomerism was modulated by changing the substitution position, offering tunable molecular planarity and π-conjugation. As a result, regulated energy levels and orbital configurations of the excited states facilitate additional TA-ISC channels as revealed by theoretical investigations. The temperature-dependent photoluminescence and fs- and ns-transient absorption spectra undoubtedly demonstrate their existence and effectiveness in promoting efficient and persistent RTP. The ISC rate constant achieves a breakthrough value of up to 1.93×10^9 s^{-1} within a poly(vinyl alcohol) matrix film, surpassing that in many existing afterglow systems containing heavy or hetero atoms. Abundant triplet excitons are populated and enable remarkable room-temperature phosphorescence performance, facilitating potential applications in constructing thermosensitive glasses and anti-counterfeiting patterns. This study offers a practical mechanism for developing novel RTP materials.

Introduction

Purely organic room-temperature phosphorescence (RTP) has emerged as a rapidly developing area in the field of organic functional materials.[1–3] Benefiting from long-lived excitons, RTP materials demonstrate promising applications including bi-oimaging, X-ray scintillators, dynamic anti-counterfeiting systems, luminescent 3D-printed constructs, and beyond.[4–9] However, achieving efficient RTP remains a pivotal challenge for purely organic phosphors due to intrinsically weak spin-forbidden intersystem crossing (ISC), which determines the upper limit of phosphorescence efficiency.[10,11] It is highly desirable to develop practical spin-flipping principles and calls for molecular design strategies to ensure the efficient ISC process.[12–14]

Recently, several rational strategies were employed to enhance spin–orbit coupling (SOC) and increase ISC efficiency, including the well-known El-Sayed rule,[15] heavy-atom effect,[16] energy gap law,[17] hyperfine coupling,[18,19] aggregation-induced level splitting,[20,21] through-space SOC,[22] second-order spin-vibronic coupling,[23] energy transfer,[24–26] and others.[27–37] Each strategy can not only effectively promote ISC channels but also creatively put forth new RTP families. However, drawbacks such as the photodegradation introduced by heteroatoms[38] and the nonradiative decay process accelerated by heavy-atoms[39] cannot be ignored. Given the importance and inconvenience of these strategies, it is of great significance to explore novel ISC principles for constructing new phosphorescent frameworks.[40]

As is well known, thermally activated reverse ISC based on donor–acceptor structures has catalyzed the rapid development of the 3rd generation of OLED materials with a thermally activated delayed fluorescence feature.[41,42] On the other hand, as a counterpart, the thermally activated forward ISC (TA-ISC) principle and related purely organic RTP have not been well investigated.[43] Several studies empirically adopt a threshold of 0.3 eV for the energy gap between S_1 and T_n states to presume both normal and thermally activated ISC.[44,45] However, compelling experimental evidence supporting endothermic TA-ISC processes from S_1 to higher-lying T_n states ($E(T_n) > E(S_1)$) in purely organic RTP systems remains notably inadequate.[46] The reason may be that the reported systems have fewer TA-ISC transition pathways and weaker spin–orbit coupling, leading to their minor contribution, which has consequently not received much attention.[43,45,47] This demonstrates that enhancing the contribution of TA-ISC to the overall ISC process

[a]School of Materials Science and Engineering, Harbin Institute of Technology Shenzhen, Shenzhen, Guangdong 518055, China. E-mail: zhangqf@hit.edu.cn; hezikai@hit.edu.cn

[b]School of Science, Harbin Institute of Technology Shenzhen, Shenzhen, Guangdong 518055, China

[c]School of Chemical Engineering and Technology, Harbin Institute of Technology, Harbin, Heilongjiang 150001, China

and exploring its potential roles hold promise for highlighting the importance of TA-ISC in the research of transition mechanisms. Modulation of the donor–acceptor architecture and control of the excited-state energy levels are expected to elucidate the excited-state pathways and regulatory mechanisms of TA-ISC.[48–50]

Herein, we developed a weakly donor–acceptor–donor (D–A–D) π-ternary system featuring varied molecular structures, tunable electronic configurations, adjustable energy levels, and persistent RTP.[51] Crucially, modulation of structural planarity was revealed to trigger additional TA-ISC pathways by increasing molecular conjugation and decreasing upper-lying triplet excited states. The π-conjugation and structural planarity of the isomers were modulated by adjusting the twisting dihedral angles, which were regulated *via* the connection position between the electron donor (carbazole) and the comparatively weak electron acceptor (dibenzothiophene) (Scheme 1). The excited states were then meticulously regulated. Suitable energy levels and orbital configurations of the excited states facilitate additional TA-ISC channels as revealed by theoretical investigations. The temperature-dependent photoluminescence and fs- and ns-transient absorption spectra undoubtedly demonstrated the existence and effectiveness of TA-ISC channels in promoting efficient and persistent RTP. Notably, the ISC rate constant achieved a breakthrough value of up to $1.93 \times 10^9\ s^{-1}$ within a poly(vinyl alcohol) film, surpassing those in typical afterglow systems containing heavy or hetero atoms[27,52,53] and facilitating abundant triplet exciton generation. In a nonradiative-decay-inhibited rigid environment, efficient RTP performance facilitated potential applications in constructing thermosensitive glasses and anti-counterfeiting luminescent patterns.

Results and discussion

In our previous work, we first proposed that the weakly D–A structure could facilitate efficient SOC through endowing a moderate singlet–triplet energy gap (ΔE_{ST}) and enhancing the LE character of excited states.[51] According to the energy gap law, small ΔE_{ST} benefits both forward and reverse nonradiative ISC. A strongly D–A structure results in the nearly degenerate lowest singlet (S_1) and triplet (T_n) excited states ($\Delta E_{ST} \sim 0$ eV). This is powerful in constructing thermally activated delayed fluorescence but not suitable for designing an efficient RTP system, because phosphorescence competes with the reverse ISC process. The weakly D–A structure can split the degenerate S_1 and T_n states (moderate ΔE_{ST}) to block the reverse ISC process. Moreover, a weakly D–A π-conjugated architecture endows the tuneable hybridized orbit configurations with charge-transfer (CT) and locally excited characteristics, allowing the El-Sayed rule and second-order vibronic coupling mechanism to work.

Following the strategy, four D–A–D molecules with different substitution modes were designed and synthesized following the procedures in Scheme 2. Carbazole (Cz) was used as the electronic donor, and dibenzothiophene (DBT) was used as the weakly electronic acceptor. The electronic donor and acceptor were assigned based on their relative electronic properties when linked within one molecular architecture, rather than their absolute electronic features. It is worth noting that Cz was lab-synthesized through a one-step coupling reaction from 2-bromodiphenylamine[54,55] to exclude the well-known impurities. The targeted compounds were synthesized *via* Ullmann coupling with moderate yields. Based on the substitution position on DBT, four molecules were named 4,6-DCzDBT, 2,8-DCzDBT, 3,7-DCzDBT, and 2,7-DCzDBT, respectively. The structural characterization and HPLC measurements are included in the SI. Further experimental details are available in the SI.

Photophysical properties

The absorption and luminescence spectra were measured to investigate the photophysical properties. As depicted in Fig. 1a, the overall absorption profiles of the four π-ternary molecules were similar, with a bathochromic shift at around 340 nm corresponding to the S_1 state. This suggested an excitation intramolecular charge transfer transition from the Cz segment to the partially conjugated DBT part. The situation aligned with the calculated HOMOs (mainly distributed at Cz units) and

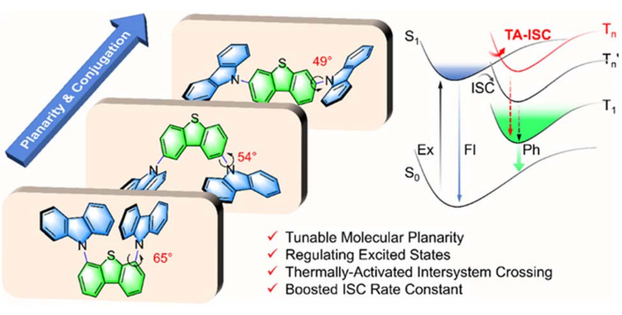

Scheme 1 Diagram of molecular structural engineering and the impact of enhanced-planarity and conjugation on intersystem crossing for achieving efficient organic RTP within a donor–acceptor–donor ternary π-conjugated framework.

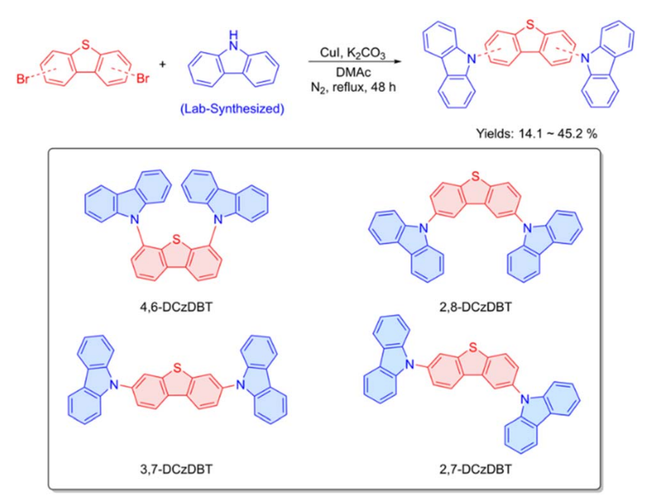

Scheme 2 Synthetic route and chemical structures of investigated ternary π-conjugated molecules.

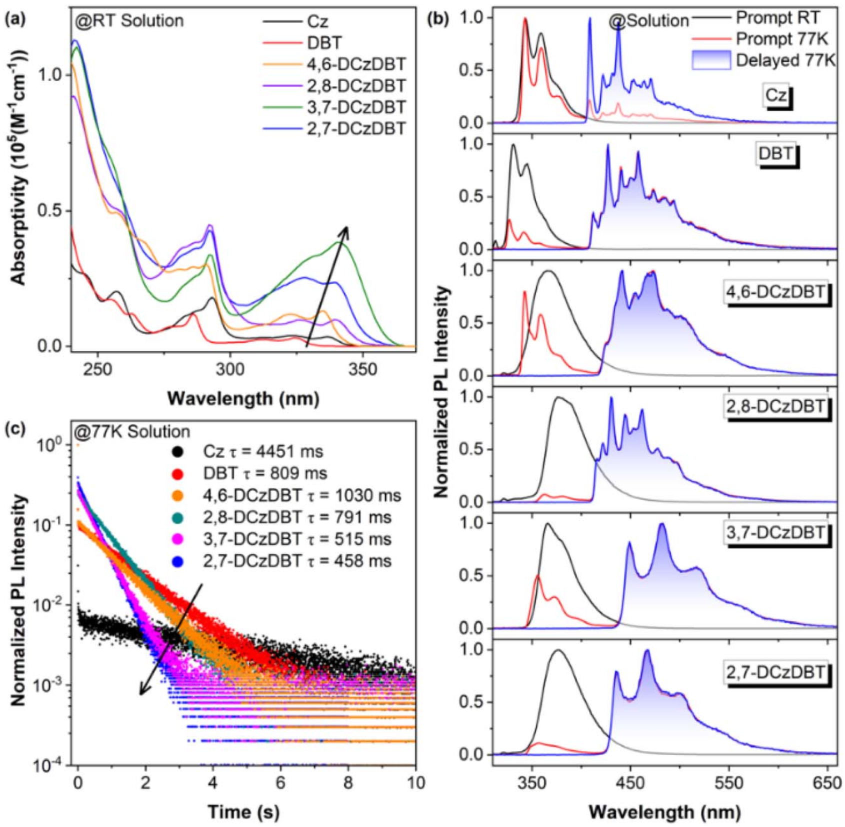

Fig. 1 (a) UV-visible absorption spectra at room temperature (RT), (b) normalized PL prompt at RT, normalized PL prompt and delayed (1 ms) spectra at 77 K under 293 nm excitation, and (c) time-resolved phosphorescent decay curves of Cz, DBT, 4,6-DCzDBT, 2,8-DCzDBT, 3,7-DCzDBT, and 2,7-DCzDBT in 2-MeTHF (10^{-5} M) at 77 K.

LUMOs (distributed at DBT units), as shown in Fig. S1, SI. The weakly D–A–D π-ternary molecular architectures were also confirmed. The absorption spectra reflected an apparent superposition of the Cz and DBT segments, together with enhanced molar absorption coefficients and redshifted onset absorption wavelengths. Specifically, 3,7-DCzDBT exhibits the longest absorption wavelength and the highest molar absorption coefficient corresponding to the S_1 excitation, indicating its superior molecular π-conjugation. In contrast, 4,6-DCzDBT displays the shortest absorption wavelength, indicating its poorest molecular π-conjugation.

Subsequently, the steady-state and delayed photoluminescence (PL) spectra were recorded (Fig. 1b). The room-temperature PL spectra displayed broad emission without vibrational progressions in contrast to the well-resolved emission profiles of the Cz and DBT segments, due to the intramolecular charge-transfer (^{1}CT) characteristics of the excited states. The nanosecond lifetimes confirmed the fluorescence nature (Table S5, SI). It is worth noting that in different solutions, the PL exhibited a polarity-dependent redshift emission behaviour, indicating the ^{1}CT characteristics of S_1 (Fig. S2, SI). Combined with the fact that the absorption spectra were hardly affected by solvent polarity, the molecules exhibit a weakly D–A–D feature at the ground state (Fig. S3, SI). This also agreed with the slightly different electronic properties of the Cz and DBT segments. When the temperature decreased to 77 K, the fluorescence emission emerged with multiple vibrational peaks similar to Cz, indicating that the fluorescence mainly originated from the Cz segments. As the temperature decreases, the conformational adjustment and feasible relaxation to a stable CT state are hindered; thus, at 77 K the system tends to exhibit the locally-excited (LE) state with vibrational PL characteristics. Simultaneously, prominent and vibrational phosphorescence emission bands emerged in the range of 420–650 nm, with lifetimes in the second range (Fig. 1c and Table S5, SI). Comparing subtle vibrational profiles (Fig. 1b) and lifetimes (Fig. 1c), it was confirmed that the phosphorescent emissions were similar to that of the DBT segment, indicating that T_1 was characterized by a dominant (π,π*) configuration contributed by the DBT segment. The weaker vibrational progressions and short persistent lifetimes in 3,7-DCzDBT and 2,7-DCzDBT were consistent with their better molecular π-conjugation. Additionally, a boosted phosphorescence proportion (the ratio of the phosphorescence emission area to the total PL spectra area) and the enhanced LE characteristics in excited states at 77 K were found in 2,8-DCzDBT and 2,7-DCzDBT, suggesting a higher ISC efficiency (Fig. S4 and S5, SI). Furthermore, the higher triplet energy level of 2,8-DCzDBT suggests that it could serve as a candidate for deep-blue emissive materials.[56] Notably, 2,7-DCzDBT combined the high phosphorescence ratio characteristic of 2,8-DCzDBT with a phosphorescence profile analogous to 3,7-DCzDBT. This demonstrated that strategic positional isomerism effectively modulated RTP performance.

After conducting fundamental photophysical property investigations in solutions, further studies were conducted on their RTP performance by polymer matrix hosting. We selected poly(vinyl alcohol) (PVA) as a rigid matrix to provide an environment for suppressed nonradiative decay, where sufficient hydroxyl groups and hydrogen bond networks inhibit intra- and intermolecular motions to trigger intrinsic molecular RTP emission.[57–60] The optimal doping mass concentration was selected as 1 : 1000 of $m_{\mathrm{Guest}} : m_{\mathrm{PVA}}$, and the as-prepared films were subjected to photothermal treatments to remove molecular oxygen and water and ensure matrix rigidity upon cross-linking (Fig. S6 and S7, SI). The PL performance of the treated PVA films was significantly improved, as illustrated in Fig. 2. Intense and persistent RTP was achieved, ascribed to the environmental rigidification. The treated films exhibit typical unimolecular emission behaviours, similar to those observed in their low-temperature solutions, but with fewer vibrational progressions. The PVA films exhibited a similar fluorescence emission band at ∼370 nm, but their phosphorescence emission differed, as illustrated by the inset pictures of Fig. 2a and the CIE coordinates in Fig. S8, SI. Unexpectedly, in contrast to the high phosphorescence ratio observed under low-temperature conditions, it is striking that 2,8-DCzDBT failed to exhibit satisfactory RTP performance. 3,7-DCzDBT and 2,7-DCzDBT exhibited outstanding afterglow performance, as confirmed by the highest quantum yield of up to 12.6% (Fig. 2c), the longer lifetime of 429 ms, and the redshifted emission wavelength in 3,7-DCzDBT films. The decay rate constants were calculated (Table S7, SI), revealing that the nonradiative decay rate constants (k_{NR}) are close for these treated PVA films, but the ISC rate constants (k_{ISC}) are distinguishable and responsible for the differentiated phosphorescence efficiencies. Notably, 3,7-DCzDBT exhibits an extremely high k_{ISC} of up to 1.93×10^9 s^{-1}, a value rarely reported for purely organic RTP systems.[22,27,52,53]

Theoretical calculations

To gain deep insights into the underlying mechanism, theoretical calculations on these molecules were performed (Fig. 3). The presented natural transition orbitals (NTOs) revealed that all molecules exhibited typical D–A–D characteristics of the S_1 state, with bilateral carbazoles acting as donors (hole) and the middle dibenzothiophene serving as the acceptor (particle). As illustrated in Fig. 3 (left), the NTOs of S_1 exhibited a main ^{1}CT character with a certain extent of ^{1}LE features, demonstrating the typical hybridized ^{1}CT and ^{1}LE nature. Concerning T_1 states, NTOs showed good orbital overlaps between holes and particles. The excited state configuration of T_1 was dominated by the

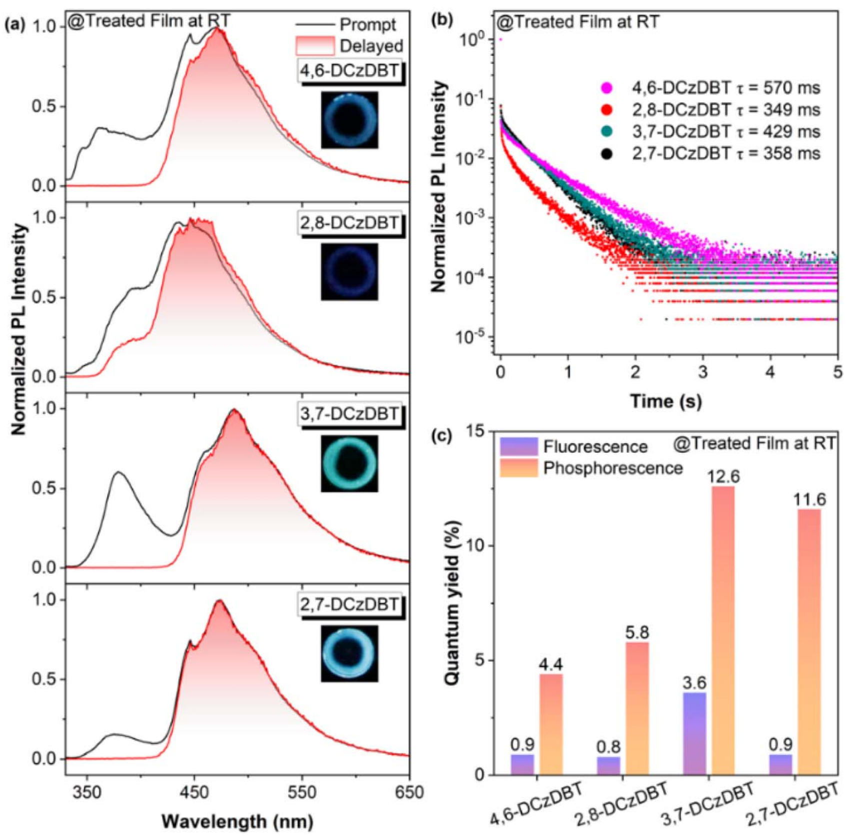

Fig. 2 (a) Normalized PL spectra and delayed (1 ms) spectra, (b) time-resolved phosphorescent decay curves, and (c) fluorescence and phosphorescence quantum yields under ambient conditions of treated PVA films with doped 4,6-DCzDBT, 2,8-DCzDBT, 3,7-DCzDBT, and 2,7-DCzDBT. Inset: photographs taken after the removal of the UV excitation source at 254 nm under ambient conditions of treated PVA films.

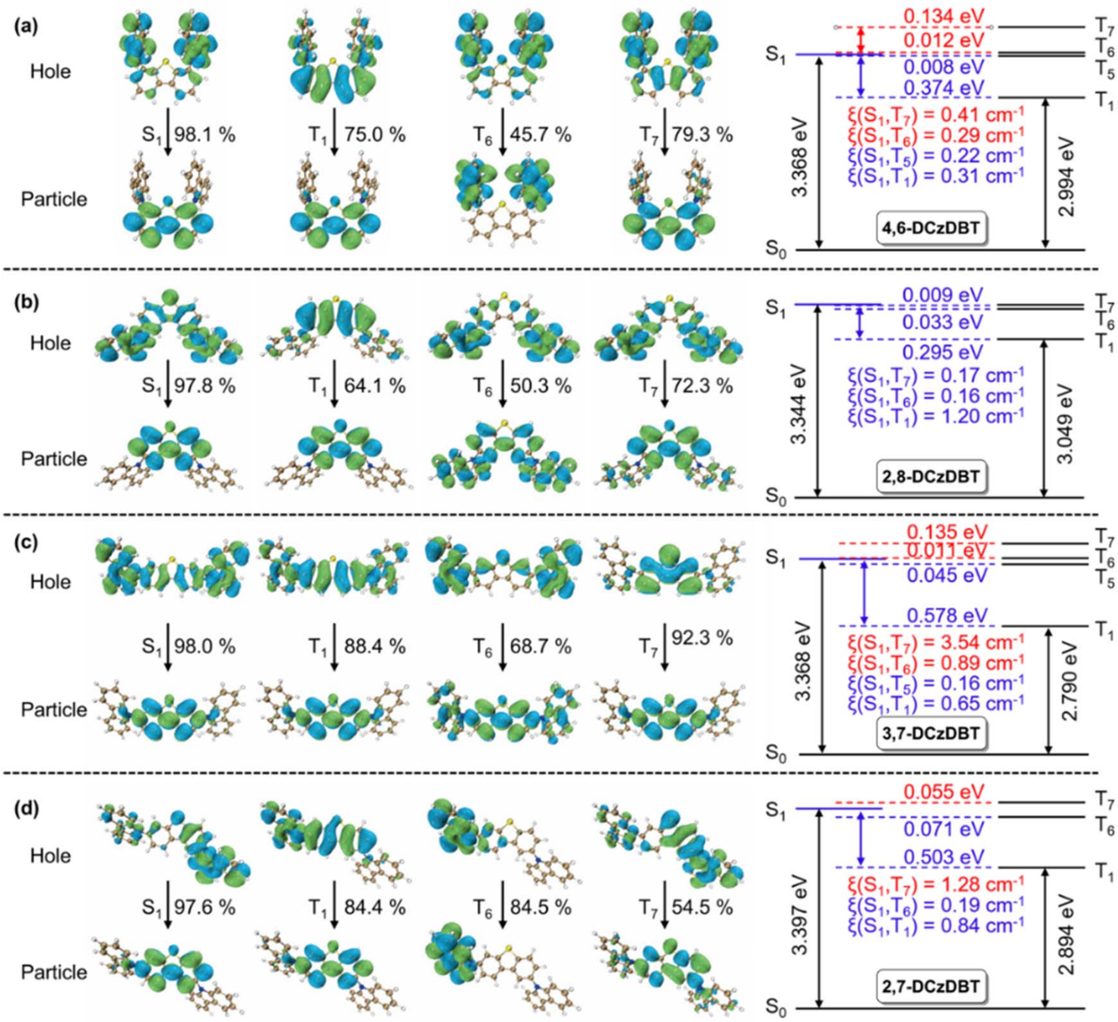

Fig. 3 The calculated natural transition orbitals of the frontier excited singlet and triplet states, the state-energy-level diagrams, and the SOC coefficients (ξ) for (a) 4,6-DCzDBT, (b) 2,8-DCzDBT, (c) 3,7-DCzDBT, and (d) 2,7-DCzDBT in the monomeric state at the (TD)-B3LYP/def2-SVP level.

^{3}LE character with little ^{3}CT feature involved. The calculation results matched well with UV-vis absorption and PL spectral profiles. Depending on the molecular structure (π-conjugation), the configuration differentiation between S_1 and T_1 can enhance the probability of the ISC transition, following El-Sayed's rule.[61] Notably, 2,8-DCzDBT has a distinct difference between the S_1 (n,π*) and T_1 (π,π*) states, resulting in a good $\xi(S_1,T_1)$ value of 1.20 cm^{-1} (Fig. 3b). However, 3,7-DCzDBT has the highest similarity of NTOs between the S_1 and T_1 states and thus a poor $\xi(S_1,T_1)$ value of 0.65 cm^{-1} (Fig. 3c). Additionally, energy gaps between S_1 and T_1 (ΔE_{ST}) indicate that the smallest ΔE_{ST} exists in 2,8-DCzDBT. Hence, 2,7-DCzDBT and 2,8-DCzDBT have stronger SOC $\xi(S_1,T_1)$ values than those of 3,7-DCzDBT and 4,6-DCzDBT. The efficient ISC was consistent with their high phosphorescence proportion in the overall PL spectra of solutions at 77 K (Fig. 1b and S5, SI).

However, upon recovering to room temperature, the RTP performance situation reversed, with 3,7-DCzDBT exhibiting outstanding afterglow performance. Therefore, further screening of the closed-lying triplet states was considered (lower than the energy level of S_2), and the possible TA-ISC processes involving multiple $S_1 \rightarrow T_n$ transition channels were found in these derivatives (Fig. 3, Tables S8 and S9, SI). Interestingly, several high SOC values were found between the higher excited triplet states (T_6 or T_7) and the S_1 state because the greater (π,π*) character in the S_1 state and the higher (n,π*) components in the T_6 and T_7 states are conducive to the ISC process. For example, 3,7-DCzDBT had two high-lying triplet excited states, T_6 (3.379 eV) and T_7 (3.503 eV), which were higher than S_1 (3.368 eV). The conspicuous NTO configurations of the main ^{3}LE feature in T_6 and T_7 supported the high values of $\xi(S_1,T_6)$ of 0.89 cm^{-1} and $\xi(S_1,T_7)$ of 3.54 cm^{-1}, respectively, despite the thermodynamically unfavourable requirements (Fig. 3c). Considering the better RTP performance of 3,7-DCzDBT and 2,7-DCzDBT, it was speculated that the high-lying triplet states of T_7 and T_6 should contribute to the overall ISC process at room temperature by providing multiple transition channels with enhanced SOC, which were absent in 2,8-DCzDBT. The endothermic process of TA-ISC from the S_1 state to the high-lying triplet states had not been experimentally verified in RTP systems, despite being occasionally mentioned.[62] The photophysical properties and calculation results inspired the possibility of involvement with the high-lying triplet states in ISC. Therefore, temperature-dependent deep photophysical investigations need to be conducted by monitoring the dynamic behaviours of excited states.

Temperature-dependent photoluminescence

As depicted in Fig. 4a and c (top), the PL spectra of the 3,7-DCzDBT doped PVA films exhibited significant temperature-dependent phosphorescence behaviours. As the temperature increased, the phosphorescence intensity initially increased from 80 to 120 K and then decreased from 140 to 320 K. It reached a maximum at 120 K by monitoring the 487 nm emission. The reduced tendency upon increasing the temperature was understandable because of the thermally enhanced non-radiative decay (k_{NR}). However, the increased tendency from 80 to 120 K was unexpected. Considering the extremely low temperature and effectively restricted molecular motions, the k_{NR} should be pretty small and does not significantly affect the system within the temperature range of 80–120 K. Therefore, the increased tendency could be attributed to the TA-ISC process and thus boost triplet exciton generation. This phenomenon is similar to the "hot triplet exciton" model observed in the high-lying reverse intersystem crossing process.[63–65] Moreover, the same phosphorescence decay curves at different temperatures eliminated the possible interferences from the anti-Kasha upper-level triplet emissions (Fig. 4b).

As shown in Fig. S9b, SI and Fig. 4c (bottom), it was observed that the phosphorescence of 2,8-DCzDBT gradually became weakened with increasing temperature, and no trend of transformation was observed. This agreed with the calculation results that there were no closed upper-lying triplet states (Fig. 3b). The apparent difference in temperature-dependent intensity trends between 3,7-DCzDBT and 2,8-DCzDBT strongly demonstrated that thermal activation played an essential role in ISC. Moreover, 4,6-DCzDBT was investigated for comparison with 3,7-DCzDBT to validate the TA-ISC process (Fig. 4d), which had a similar energy gap between S_1 and T_7 but different SOC values. As the temperature decreased, the phosphorescence intensity gradually increased due to the reduction of k_{NR}. However, at around 150 K, a gentle downward slope appeared, indicating the involvement of upper-level triplet state T_7 in the ISC process. Unfortunately, the small SOC value

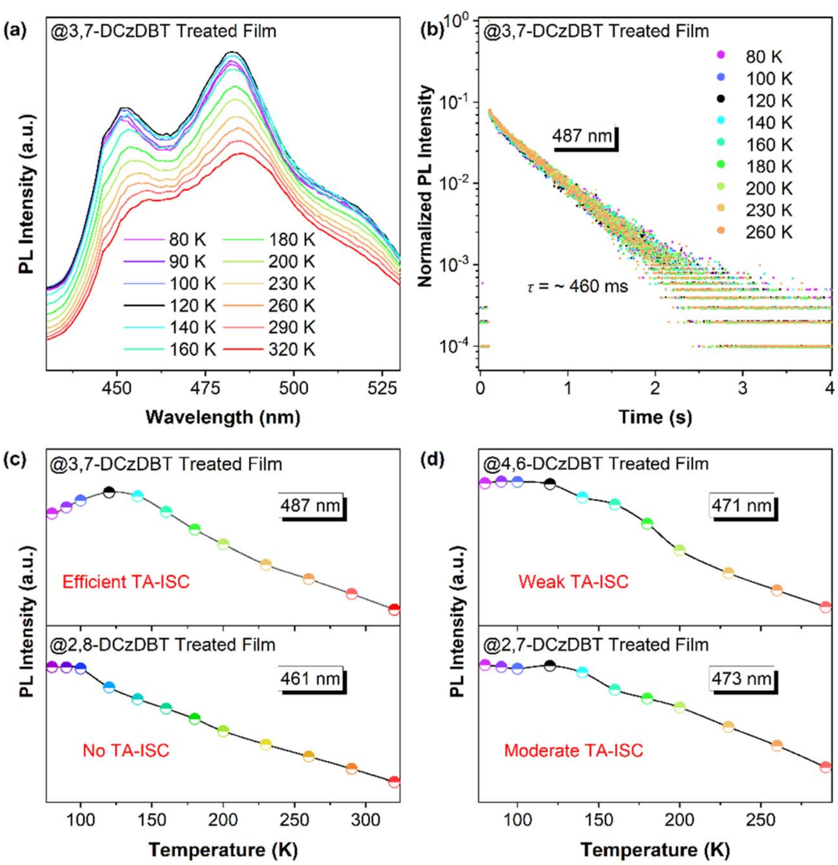

Fig. 4 (a) Phosphorescence spectra and (b) time-resolved phosphorescent decay curves at different temperatures of the treated PVA films with doped 3,7-DCzDBT. The emission intensity of maximum emission peaks at different temperatures of (c) 3,7-DCzDBT and 2,8-DCzDBT, and (d) 4,6-DCzDBT and 2,7-DCzDBT.

$\xi(S_1,T_7)$ exerted a weaker effect on the overall ISC process; a similar increased tendency was not observed (Fig. S9a, SI). We also characterized the temperature-dependent PL spectra of 2,7-DCzDBT, as shown in Fig. S9c, SI and Fig. 4d (bottom). Similar to 3,7-DCzDBT, the temperature-dependent phosphorescence intensity curve of 2,7-DCzDBT showed a trend shift at around 120 K, which was consistent with the calculated results. The temperature-dependent PL spectra and calculated results consistently confirmed the existence of the TA-ISC process. The significant contribution of the upper-level triplet excited states in populating the emissive T_1 excitons was revealed.

Temperature-dependent transient absorption

To elucidate the underlying photophysical mechanisms of the singlet–triplet transition, we employed transient absorption (TA) spectroscopy to probe the excited-state evolution dynamics of the representative 2,8-DCzDBT and 3,7-DCzDBT.[66,67] First, femtosecond transient absorption (fs-TA) measurements revealed a positive signal in the range of 500–700 nm for both systems (Fig. 5a and b), indicative of excited-state absorption (ESA) corresponding to $S_1 \rightarrow S_n$ transitions. TA wavelength kinetic traces were extracted to resolve the state-specific dynamics. For 3,7-DCzDBT, the ESA signal reached its maximum intensity within 594 fs and decayed with the S_1 relaxation, consistent with its fluorescence lifetime as monitored at 575 nm ($\tau = 0.3$ ns) (Fig. 5c and Table S5, SI). An analogous decay was observed for 2,8-DCzDBT at 620 nm (Fig. S10c, SI). Notably, a distinct transient signal rather than noise emerged at ~1000 ps. Its intensity underwent the complete rise–decay profile and was found to be stronger when monitored at 650 nm than at 575 nm (Fig. 5c inset). Later on, it was assigned to triplet–triplet absorption (TTA) from the upper-level T_7 state with a nanosecond decay lifetime (~0.7 ns), indicating the presence of $S_1 \rightarrow T_n$ TA-ISC transitions. There is no corresponding feature detected in 2,8-DCzDBT (Fig. S10c, SI).

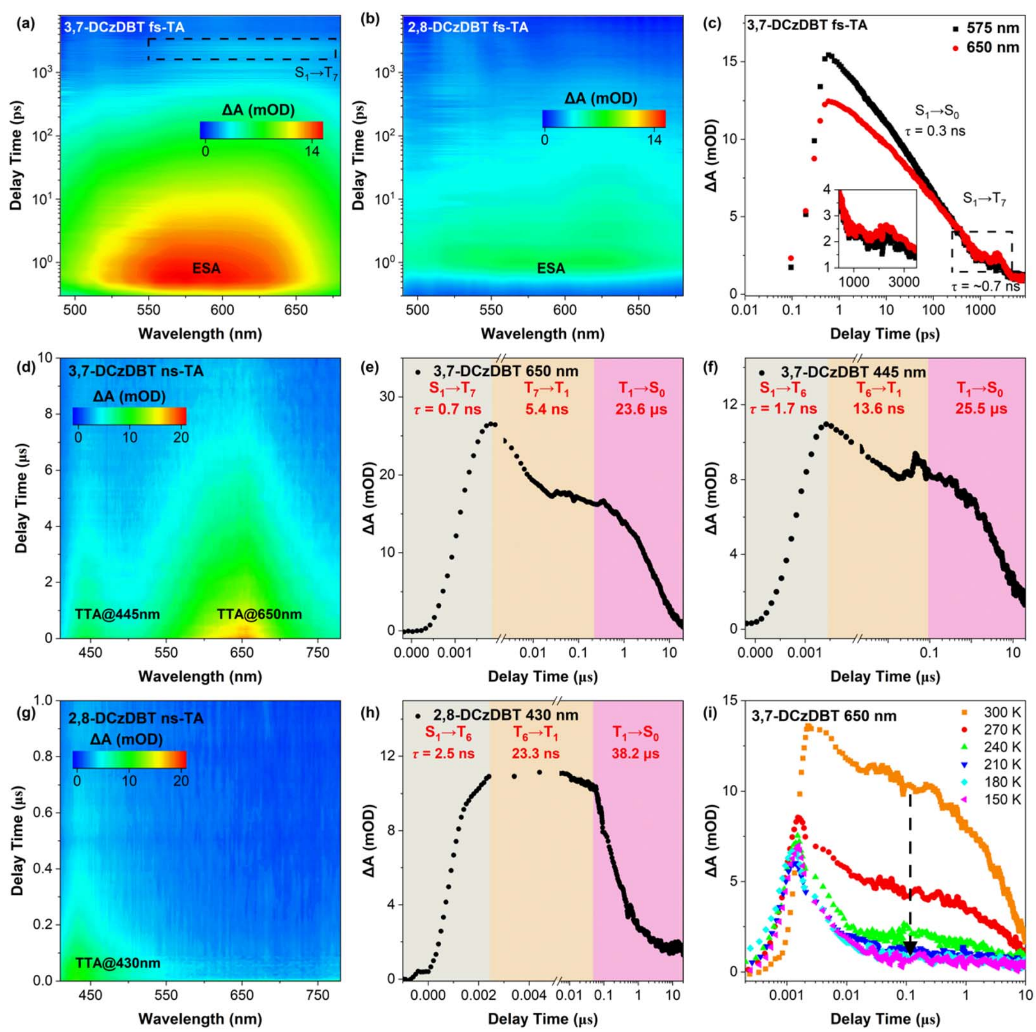

Fig. 5 Decay time-wavelength two-dimensional fs-TA color maps of (a) 3,7-DCzDBT and (b) 2,8-DCzDBT, and ns-TA color maps of (d) 3,7-DCzDBT and (g) 2,8-DCzDBT in 2-MeTHF (10^{-4} M) at room temperature. (c) fs-TA dynamics detected at 575 and 650 nm in 3,7-DCzDBT. ns-TA dynamics detected at (e) 650 nm and (f) 445 nm in 3,7-DCzDBT, and (h) 430 nm in 2,8-DCzDBT, respectively, with the corresponding excited-state relaxation lifetimes. (i) ns-TA dynamics at different temperatures from 300 to 150 K detected at 650 nm in 3,7-DCzDBT. The pump light wavelength is 340 nm.

To elucidate the dynamics of triplet states, nanosecond transient absorption (ns-TA) spectroscopy was then performed on 2,8-DCzDBT and 3,7-DCzDBT (Fig. 5d and g). Distinctly, 3,7-DCzDBT exhibited dual absorption bands at around 400–500 nm (TTA@445 nm) and 550–750 nm (TTA@650 nm), respectively, in contrast to the one absorption band in the range of 400–500 nm in 2,8-DCzDBT (TTA@430 nm). Kinetic traces extracted from these bands displayed microsecond-scale decays, confirming triplet exciton-mediated processes and indicating their TTA features (Fig. 5e, f, and h). Multi-exponential analysis revealed complex rise–decay profiles indicative of step relaxation. Cross-validation ns-TA with NTO calculations and photoluminescence data enabled dynamics assignments: for 3,7-DCzDBT absorption at 650 nm (Fig. 5e), an initial rise component ($\tau = 0.7$ ns) directly signified $S_1 \rightarrow T_7$ TA-ISC, being consistent with the fs-TA ESA signal in Fig. 5c and the calculated k_{ISC} based on steady-state photophysical properties (1.93×10^9 s^{-1}), followed by a rapid decay ($\tau = 5.4$ ns) attributed to $T_7 \rightarrow T_1$ internal conversion, culminating in a slow decay ($\tau = 23.6$ μs) corresponding to $T_1 \rightarrow S_0$ depopulation. The band corresponded to the TA from the upper level T_7 state. Analogous dynamics at 445 nm (Fig. 5f) involved a slower $S_1 \rightarrow T_6$ normal ISC ($\tau = 1.7$ ns) with a subsequent $T_6 \rightarrow T_1$ internal conversion ($\tau = 13.6$ ns) and a $T_1 \rightarrow S_0$ depopulation with a similar decay lifetime of 25.5 μs. Critically, ns-TA in Fig. 5d confirmed $S_1 \rightarrow T_7$ TA-ISC as the dominant evolution pathway in 3,7-DCzDBT, consistent with theoretical predictions.

In contrast, ns-TA of 2,8-DCzDBT at 430 nm (Fig. 5g and h) demonstrated the evolution process of the $S_1 \rightarrow T_6$ ISC ($\tau = 2.5$ ns, notably longer than 0.7 ns in 3,7-DCzDBT), the $T_6 \rightarrow T_1$ internal conversion, and the $T_1 \rightarrow S_0$ depopulation ($\tau = 38.2$ μs), with no spectroscopic evidence for upper-level T_7 involvement. The kinetic difference that accelerated ISC and shortened T_1 decay in 3,7-DCzDBT relative to 2,8-DCzDBT directly rationalized the observed different RTP behaviours. To further validate TA-ISC, temperature-dependent ns-TA measurements were conducted (Fig. 5i and S10, SI). For 3,7-DCzDBT, the ns-TA signal intensity at 650 nm progressively diminished with decreasing temperature, indicating the suppression or absence of $S_1 \rightarrow T_7$ ISC channels at low temperature. No appreciable signal variations occurred in 2,8-DCzDBT at 445 nm (Fig. S10b, SI). Nevertheless, the cumulative evidence confirmed not only the existence of TA-ISC but also its superior capability of promoting ISC in 3,7-DCzDBT.

Structure–property relationship

It is crucial to scrutinize the underlying structure–property relationship and formulate a rational molecular design strategy to develop TA-ISC RTP systems. π-Conjugation, the degree of π-electron delocalization, corresponds to the molecular planarity and substitution-dependent electronic effects in these polycyclic aromatic structures. Based on the extent of redshift absorption, π-conjugation suggests an ordered and increased molecular planarity from 4,6-DCzDBT to 2,8-DCzDBT, 2,7-DCzDBT, and 3,7-DCzDBT. Their molecular configurations were then obtained by growing single crystals and were doubly verified by theoretical calculations. As shown in Fig. 6a, the calculated molecular structures closely resembled those of the single crystals, particularly in terms of the dihedral angles between the carbazole and dibenzothiophene units. The subtle discrepancies in the dihedral angles arise from the compression or deformation of the molecular conformation within the unit cell due to intermolecular interactions. Notably, 4,6-DCzDBT possessed the largest dihedral angles, and 3,7-DCzDBT represented the smallest dihedral angles. The small dihedral angles indicated high molecular planarity and π-conjugation, which aligned with the redshifted emission wavelength and their superior RTP performance (Fig. 2c). In detail, the high molecular planarity of 3,7-DCzDBT lowered energy levels of the upper triplet states through enhanced π-conjugation, allowing upper-level T_7 to approach S_1 and facilitating the TA-ISC process. Additionally, enhanced π-conjugation supported T_7 in providing more ^{3}LE configurations on the central emitting DBT acceptor, and the ^{3}LE configuration promoted efficient TA-ISC by fulfilling El-Sayed's rule between hybridized S_1 (^{1}CT + ^{1}LE) and T_7 (^{3}LE). It is worth noting that 2,7-DCzDBT inherited partial structural and conjugation characteristics from its 2,8-DCzDBT and 3,7-DCzDBT counterparts, demonstrating intermediate RTP performance in terms of lifetime (close to that of 2,8-DCzDBT) and efficiency (close to that of 3,7-DCzDBT) (Fig. 2).

Therefore, the precise control of molecular π-conjugation in the weakly D–A–D system can finely tune the ISC process and facilitate RTP performance accordingly. When a large dihedral angle existed between the π-donor and π-acceptor, the singlet and triplet excited states possessed weak SOC and insufficient ISC due to the same orbital configurations. Through enhancing structural planarity by reducing large dihedral angles, the delocalization within the donor–acceptor structure regulated the electronic configuration of the excited states. The energy level of the upper triplet excited states was lowered, and the orbital configuration of the close-lying triplet state was converted. As a result, additional TA-ISC channels with high SOC values were facilitated, boosting RTP efficiency (Fig. 6b). As a benefit, the high π-conjugation provided a relatively pure (π,π*) configuration for T_1, guaranteeing a small radiative rate of phosphorescence and, consequently, a persistent RTP lifetime. These findings not only provide us with a clear and practical molecular design principle but also yield high-performance phosphors.

Anti-counterfeiting and thermal sensing applications

Given the remarkable phosphorescence performance of these doped PVA films, we explored their applications in anti-counterfeiting and thermal sensing as a proof of concept. As depicted in Fig. 7a, treated PVA films containing 3,7-DCzDBT and 2,7-DCzDBT were utilized to construct a simple anti-counterfeiting pattern of “HIT”. Upon UV excitation, the luminescent pattern was observed. When the excitation ceased, an afterglow pattern of “HIT” persisted. Two seconds later, the pattern transformed to the “1111” pattern. In addition, a peach-shaped PVA film doped with 3,7-DCzDBT was soaked and

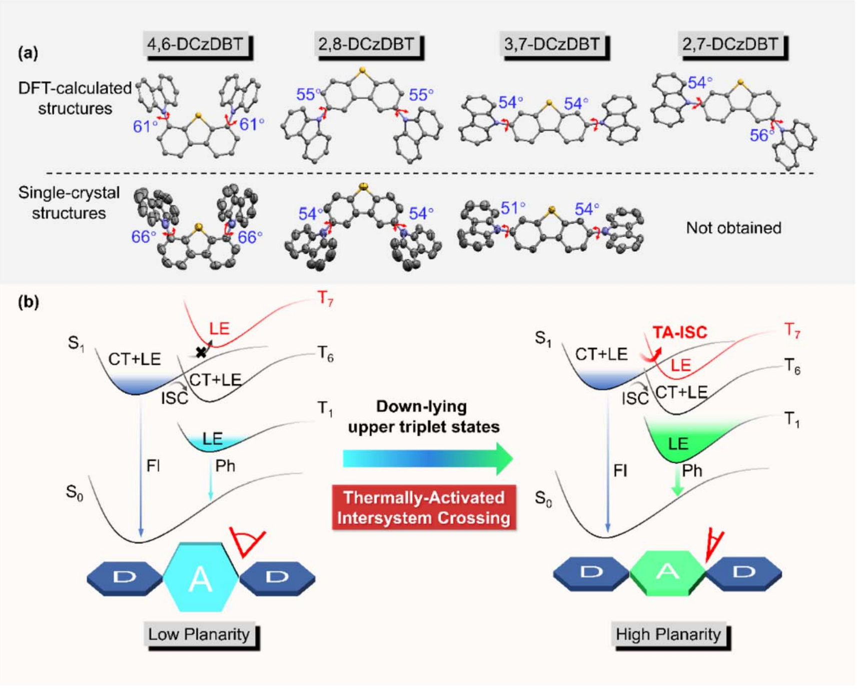

Fig. 6 (a) Single-crystal structures and density functional theory (DFT) optimized structures of 4,6-DCzDBT, 2,8-DCzDBT, 3,7-DCzDBT, and 2,7-DCzDBT with average-calculated dihedral angles between carbazole and dibenzothiophene units. (b) Schematic diagram describing the thermally activated ISC principle.

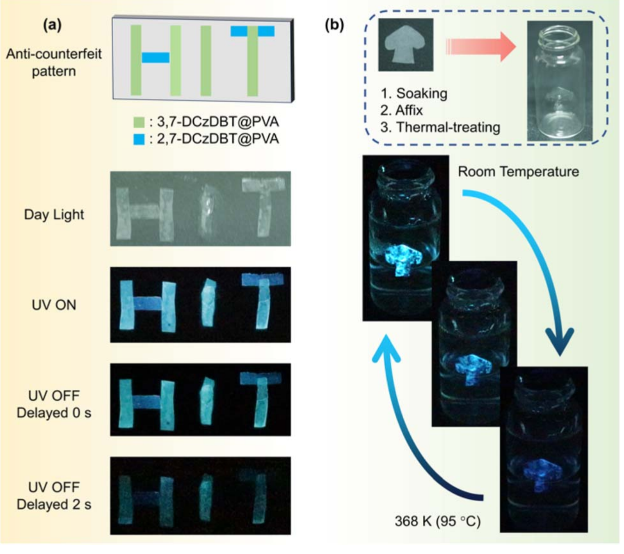

Fig. 7 (a) Schematic diagram of the preparation of anti-counterfeiting patterns and photographs of the security code before and after turning off the 254 nm UV lamp. (b) Schematic diagram of the preparation of thermosensitive glasses with a 3,7-DCzDBT film and pictures of the thermal-sensing process from 368 K to 295 K under 254 nm UV lamp excitation.

affixed to glass bottles, followed by a 40 minutes thermal treatment (Fig. 7b). The prepared film was employed to monitor the environmental temperature. It was observed that as the temperature increased (368 K), the colour gradually shifted to deep blue, and the brightness decreased. Subsequently, as the temperature dropped, the emission was restored to its initial state. The process can be repeated for several cycles.

Conclusion

In summary, we have successfully developed a weakly donor–acceptor–donor π-conjugated system featuring isomerism-dependent RTP characteristics. The substitution mode exerted a notable influence on molecular planarity and π-conjugation, enabling precise control over the excited-state characteristics. Down-lying upper triplet excited states introduce additional TA-ISC channels as revealed by theoretical investigations and proved by temperature-dependent photoluminescence and fs- and ns-transient absorption spectra. As a result, the overall ISC rate constant has reached a remarkable value of $1.93 \times 10^9\ s^{-1}$. It is worth noting that the principle of TA-ISC is in its infancy, but it is a practical mechanism for developing novel RTP materials and deserves further investigation.

Author contributions

W. H. performed all photophysical measurements, analysed the data, synthesized the materials, and grew the crystals. Y. Z. and C. W. performed the theoretical calculations. K. Z. assisted in the analysis of molecular crystal structures. Z. H. and Q. Z. designed and supervised the research and revised the manuscript. All authors discussed the results and commented on the manuscript.

Conflicts of interest

There are no conflicts to declare.

Data availability

Supplementary information: materials, instruments, synthetic and experimental procedures, and characterization data. See DOI: **https://doi.org/10.1039/d5sc07119d**.

Acknowledgements

The authors acknowledge the financial support from the National Natural Science Foundation of China (No. 22375054 and No. 21975061), the Natural Science Foundation of Guangdong Province (No. 2024B15150200960), the Shenzhen Fundamental Research Program (No. JCYJ20241202152659001 and No. GXWD20231130104319001), and the Postdoctoral Fellowship Program (Grade C) of the China Postdoctoral Science Foundation (No. GZC20252722). The authors thank Dr Kang Zhou (Shenzhen Polytechnic University) for single-crystal structure analysis.

References

1 W. Zhao, Z. He and B. Z. Tang, Room-temperature phosphorescence from organic aggregates, *Nat. Rev. Mater.*, 2020, **5**, 869–885.
2 B. Zhou and D. Yan, Long Persistent Luminescence from Metal-Organic Compounds: State of the Art, *Adv. Funct. Mater.*, 2023, **33**, 2300735.
3 W. Huang and Z. He, Initialing circularly polarized room-temperature phosphorescence from purely organic luminophore aggregate, *Synlett*, 2023, **34**, 2249–2256.
4 S. M. A. Fateminia, Z. Mao, S. Xu, Z. Yang, Z. Chi and B. Liu, Organic Nanocrystals with Bright Red Persistent Room-Temperature Phosphorescence for Biological Applications, *Angew. Chem., Int. Ed.*, 2017, **56**, 12160–12164.
5 Z. Tian, D. Li, E. V. Ushakova, V. G. Maslov, D. Zhou, P. Jing, D. Shen, S. Qu and A. L. Rogach, Multilevel Data Encryption Using Thermal-Treatment Controlled Room Temperature Phosphorescence of Carbon Dot/Polyvinylalcohol Composites, *Adv. Sci.*, 2018, **5**, 1800795.
6 H. F. Higginbotham, M. Okazaki, P. de Silva, S. Minakata, Y. Takeda and P. Data, Heavy-Atom-Free Room-Temperature Phosphorescent Organic Light-Emitting Diodes Enabled by Excited States Engineering, *ACS Appl. Mater. Interfaces*, 2021, **13**, 2899–2907.
7 Z. Wu, J. Nitsch and T. B. Marder, Persistent Room-Temperature Phosphorescence from Purely Organic Molecules and Multi-Component Systems, *Adv. Opt. Mater.*, 2021, **9**, 2100411.
8 N. Gan, X. Zou, M. Dong, Y. Wang, X. Wang, A. Lv, Z. Song, Y. Zhang, W. Gong, Z. Zhao, Z. Wang, Z. Zhou, H. Ma, X. Liu, Q. Chen, H. Shi, H. Yang, L. Gu, Z. An and W. Huang, Organic phosphorescent scintillation from copolymers by X-ray irradiation, *Nat. Commun.*, 2022, **13**, 3995.
9 Z. Huang, Z. He, B. Ding, H. Tian and X. Ma, Photoprogrammable Circularly Polarized Phosphorescence Switching of Chiral Helical Polyacetylene Thin Films, *Nat. Commun.*, 2022, **13**, 7841.
10 W. Shao and J. Kim, Metal-free organic phosphors toward fast and efficient room-temperature phosphorescence, *Acc. Chem. Res.*, 2022, **55**, 1573–1585.
11 H. Shi, W. Yao, W. Ye, H. Ma, W. Huang and Z. An, Ultralong Organic Phosphorescence: From Material Design to Applications, *Acc. Chem. Res.*, 2022, **55**, 3445–3459.
12 R. R. Valiev, V. N. Cherepanov, R. T. Nasibullin, D. Sundholm and T. Kurten, Calculating rate constants for intersystem crossing and internal conversion in the Franck-Condon and Herzberg-Teller approximations, *Phys. Chem. Chem. Phys.*, 2019, **21**, 18495–18500.
13 M. Lv, Y. Yu, M. E. Sandoval-Salinas, J. Xu, Z. Lei, D. Casanova, Y. Yang and J. Chen, Engineering the Charge-Transfer State to Facilitate Spin-Orbit Charge Transfer Intersystem Crossing in Spirobis[anthracene]diones, *Angew. Chem., Int. Ed.*, 2020, **59**, 22179–22184.
14 C. M. Marian, Understanding and Controlling Intersystem Crossing in Molecules, *Annu. Rev. Phys. Chem.*, 2021, **72**, 617–640.
15 B. Wu, H. Su, A. Cheng, X. Zhang, T. Wang and G. Zhang, The El-Sayed's rule analogy enables long-lived room temperature phosphorescence in twisted biphenyls, *Cell Rep. Phys. Sci.*, 2023, **4**, 101245.
16 Y. He, J. Wang, Q. Li, S. Qu, C. Zhou, C. Yin, H. Ma, H. Shi, Z. Meng and Z. An, Highly Efficient Room-Temperature Phosphorescence Promoted via Intramolecular-Space Heavy-Atom Effect, *Adv. Opt. Mater.*, 2023, **11**, 2201641.
17 Y. Zhou, L. Qu, S. Yi, C. Wang, X. Chen, S. Tang, H. Tang, Y. Li, K. Wang, Y. Zhao and C. Yang, Dual Promotion of Phosphorus Groups for Ultralong Room Temperature Phosphorescence with High Efficiency, *Adv. Opt. Mater.*, 2022, **11**, 2201904.
18 S. Kuno, T. Kanamori, Z. Yijing, H. Ohtani and H. Yuasa, Long Persistent Phosphorescence of Crystalline Phenylboronic Acid Derivatives: Photophysics and a Mechanistic Study, *ChemPhotoChem*, 2017, **1**, 102–106.
19 J. T. Buck, A. M. Boudreau, A. DeCarmine, R. W. Wilson, J. Hampsey and T. Mani, Spin-Allowed Transitions Control the Formation of Triplet Excited States in Orthogonal Donor-Acceptor Dyads, *Chem*, 2019, **5**, 138–155.
20 L. Zhang, M. Li, Q.-Y. Gao and C.-F. Chen, An ultralong room-temperature phosphorescent material based on the combination of small singlet–triplet splitting energy and H-aggregation, *Chem. Commun.*, 2020, **56**, 4296–4299.
21 M. Park, H. S. Kim, H. Yoon, J. Kim, S. Lee, S. Yoo and S. Jeon, Controllable Singlet-Triplet Energy Splitting of Graphene Quantum Dots through Oxidation: From Phosphorescence to TADF, *Adv. Mater.*, 2020, **32**, 2000936.
22 J. Yu, H. Ma, W. Huang, Z. Liang, K. Zhou, A. Lv, X. G. Li and Z. He, Purely Organic Room-Temperature Phosphorescence

Endowing Fast Intersystem Crossing from Through-Space Spin-Orbit Coupling, *JACS Au*, 2021, **1**, 1694–1699.

23 M. K. Etherington, J. Gibson, H. F. Higginbotham, T. J. Penfold and A. P. Monkman, Revealing the spin-vibronic coupling mechanism of thermally activated delayed fluorescence, *Nat. Commun.*, 2016, **7**, 13680.

24 Y. Wang, J. Yang, M. Fang, Y. Yu, B. Zou, L. Wang, Y. Tian, J. Cheng, B. Z. Tang and Z. Li, Förster Resonance Energy Transfer: An Efficient Way to Develop Stimulus-Responsive Room-Temperature Phosphorescence Materials and Their Applications, *Matter*, 2020, **3**, 449–463.

25 F.-F. Shen, Y. Chen, X. Dai, H.-Y. Zhang, B. Zhang, Y. Liu and Y. Liu, Purely organic light-harvesting phosphorescence energy transfer by β-cyclodextrin pseudorotaxane for mitochondria targeted imaging, *Chem. Sci.*, 2021, **12**, 1851–1857.

26 W. Xie, W. Huang, J. Li, Z. He, G. Huang, B. S. Li and B. Z. Tang, Anti-Kasha triplet energy transfer and excitation wavelength dependent persistent luminescence from host-guest doping systems, *Nat. Commun.*, 2023, **14**, 8098.

27 Y. Tao, R. Chen, H. Li, J. Yuan, Y. Wan, H. Jiang, C. Chen, Y. Si, C. Zheng, B. Yang, G. Xing and W. Huang, Resonance-Activated Spin-Flipping for Efficient Organic Ultralong Room-Temperature Phosphorescence, *Adv. Mater.*, 2018, **30**, 1803856.

28 Y. Tao, C. Liu, Y. Xiang, Z. Wang, X. Xue, P. Li, H. Li, G. Xie, W. Huang and R. Chen, Resonance-Induced Stimuli-Responsive Capacity Modulation of Organic Ultralong Room Temperature Phosphorescence, *J. Am. Chem. Soc.*, 2022, **144**, 6946–6953.

29 S. Garain, S. Sarkar, B. C. Garain, S. K. Pati and S. J. George, Chiral Arylene Diimide Phosphors: Circularly Polarized Ambient Phosphorescence from Bischromophoric Pyromellitic Diimides, *Angew. Chem., Int. Ed.*, 2022, **61**, e202115773.

30 H. Su, K. Hu, W. Huang, T. Wang, X. Zhang, B. Chen, H. Miao, X. Zhang and G. Zhang, Functional Roles of Polymers in Room-Temperature Phosphorescent Materials: Modulation of Intersystem Crossing, Air Sensitivity and Biological Activity, *Angew. Chem., Int. Ed.*, 2023, **62**, e202218712.

31 W. Huang, C. Fu, Z. Liang, K. Zhou and Z. He, Strong Circularly-Polarized Room-Temperature Phosphorescence from a Feasibly Separable Scaffold of Bidibenzo[b,d]furan with Locked Axial Chirality, *Angew. Chem., Int. Ed.*, 2022, **61**, e202202977.

32 Q. Jia, X. Yan, B. Wang, J. Li, W. Xu, Z. Shen, C. Bo, Y. Li and L. Chen, Construction of room temperature phosphorescent materials with ultralong lifetime by in-situ derivation strategy, *Nat. Commun.*, 2023, **14**, 7164.

33 E. Bassan, A. Gualandi, P. G. Cozzi and P. Ceroni, Design of BODIPY dyes as triplet photosensitizers: electronic properties tailored for solar energy conversion, photoredox catalysis and photodynamic therapy, *Chem. Sci.*, 2021, **12**, 6607–6628.

34 Y. Dong, A. Elmali, J. Zhao, B. Dick and A. Karatay, Long-Lived Triplet Excited State Accessed with Spin–Orbit Charge Transfer Intersystem Crossing in Red Light-Absorbing Phenoxazine-Styryl BODIPY Electron Donor/Acceptor Dyads, *ChemPhysChem*, 2020, **21**, 1388–1401.

35 Y. Zhang, Q. Sun, J. Chen, S. Cui, H. Zhang, S. Xue and W. Yang, Evoking ultra-long molecular room temperature phosphorescence of pure carbazole derivatives, *Chem. Eng. J.*, 2022, **447**, 137458.

36 S. Garain, S. N. Ansari, A. A. Kongasseri, B. C. Garain, S. K. Pati and S. J. George, Room temperature charge-transfer phosphorescence from organic donor-acceptor Co-crystals, *Chem. Sci.*, 2022, **13**, 10011–10019.

37 W. Huang, Y. Zhu, K. Zhou, L. Chen, Z. Zhao, E. Zhao and Z. He, Boosting Circularly Polarized Luminescence from Alkyl-Locked Axial Chirality Scaffold by Restriction of Molecular Motions, *Chem.–Eur. J.*, 2024, **30**, e202303667.

38 J. Ma, X. Zhang and D. L. Phillips, Time-Resolved Spectroscopic Observation and Characterization of Water-Assisted Photoredox Reactions of Selected Aromatic Carbonyl Compounds, *Acc. Chem. Res.*, 2019, **52**, 726–737.

39 J. Zhou, L. Stojanović, A. A. Berezin, T. Battisti, A. Gill, B. M. Kariuki, D. Bonifazi, R. Crespo-Otero, M. R. Wasielewski and Y.-L. Wu, Organic room-temperature phosphorescence from halogen-bonded organic frameworks: hidden electronic effects in rigidified chromophores, *Chem. Sci.*, 2021, **12**, 767–773.

40 Y. Ma, Y. Yu, J. Li, S. Liu, W. Huang and Q. Zhao, Stimuli-responsive photofunctional materials for green and security printing, *InfoMat*, 2021, **3**, 82–100.

41 H. Uoyama, K. Goushi, K. Shizu, H. Nomura and C. Adachi, Highly efficient organic light-emitting diodes from delayed fluorescence, *Nature*, 2012, **492**, 234–238.

42 Y. Wada, H. Nakagawa, S. Matsumoto, Y. Wakisaka and H. Kaji, Organic light emitters exhibiting very fast reverse intersystem crossing, *Nat. Photonics*, 2020, **14**, 643–649.

43 L. Deng, Z. Ma, J. Zhou, L. Chen, J. Wang, X. Qiao, D. Hu, D. Ma, J. Peng and Y. Ma, Regulating excited state of sulfone-locked triphenylamine heteroaromatics for high-efficiency ultralong room-temperature phosphorescence, *Chem. Eng. J.*, 2022, **449**, 137834.

44 H. Yang, Y. Wang, X. Yao, H. Ma, J. Yu, X. Li, X. Wang, X. Liang, Q. Peng, S. Cai, Z. An and W. Huang, Efficient and Ultralong Room Temperature Phosphorescence from Isolated Molecules under Visible Light Excitation, *J. Am. Chem. Soc.*, 2025, **147**, 1474–1481.

45 Y. Xiao, J. Li, Z. Song, J. Liao, M. Shen, T. Yu and W. Huang, 3D Printable Materials with Visible Light Triggered Photochromism and Room Temperature Phosphorescence, *J. Am. Chem. Soc.*, 2025, **147**, 20372–20380.

46 R. G. Bennett and P. J. McCartin, Radiationless Deactivation of the Fluorescent State of Substituted Anthracenes, *J. Chem. Phys.*, 1966, **44**, 1969–1972.

47 X. Han, H.-Q. Zheng, Y. Yang, Y. Cui and G. Qian, Tunable Room-Temperature Phosphorescence in Hydrogen-Bonded Organic Crystals via H-Bonding Units, *Adv. Funct. Mater.*, 2025, **35**, 2425934.

48 D. Dou, X. Zhou, T. Wang, Q. Yang, X. Tan, Z. Ling, M. Manz, X. Liu, G.-J. A. H. Wetzelaer, X. Li, M. Baumgarten, P. W. M. Blom and Y. Li, Intramolecular Through-Space Charge-Transfer Effect for Achieving Room-Temperature Phosphorescence in Amorphous Film, *Adv. Opt. Mater.*, 2024, **12**, 2400976.

49 X. Liu, L. Yang, X. Li, L. Zhao, S. Wang, Z.-H. Lu, J. Ding and L. Wang, An Electroactive Pure Organic Room-Temperature Phosphorescence Polymer Based on a Donor-Oxygen-Acceptor Geometry, *Angew. Chem., Int. Ed.*, 2021, **60**, 2455–2463.

50 T. Wang, Z. Hu, X. Nie, L. Huang, M. Hui, X. Sun and G. Zhang, Thermochromic aggregation-induced dual phosphorescence via temperature-dependent sp3-linked donor-acceptor electronic coupling, *Nat. Commun.*, 2021, **12**, 1364.

51 W. Huang, Y. Zhu, X. Xie, G. Tang, K. Zhou, L. Song and Z. He, Utilizing weakly donor-acceptor ternary pi-conjugated architecture to achieve single-component white luminescence and stimulus-responsive room-temperature phosphorescence, *Chem. Sci.*, 2024, **15**, 12316–12325.

52 W. Dai, X. Niu, X. Wu, Y. Ren, Y. Zhang, G. Li, H. Su, Y. Lei, J. Xiao, J. Shi, B. Tong, Z. Cai and Y. Dong, Halogen Bonding: A New Platform for Achieving Multi-Stimuli-Responsive Persistent Phosphorescence, *Angew. Chem., Int. Ed.*, 2022, **61**, e202200236.

53 Z. Wu, J. Nitsch, J. Schuster, A. Friedrich, K. Edkins, M. Loebnitz, F. Dinkelbach, V. Stepanenko, F. Würthner, C. M. Marian, L. Ji and T. B. Marder, Persistent Room Temperature Phosphorescence from Triarylboranes: A Combined Experimental and Theoretical Study, *Angew. Chem., Int. Ed.*, 2020, **59**, 17137–17144.

54 C. Chen, Z. Chi, K. C. Chong, A. S. Batsanov, Z. Yang, Z. Mao, Z. Yang and B. Liu, Carbazole isomers induce ultralong organic phosphorescence, *Nat. Mater.*, 2021, **20**, 175–180.

55 J. Song, Y. Wang, L. Qu, L. Fang, X. Zhou, Z.-X. Xu, C. Yang, P. Wu and H. Xiang, Room-Temperature Phosphorescence of Pure Axially Chiral Bicarbazoles, *J. Phys. Chem. Lett.*, 2022, **13**, 5838–5844.

56 S. H. Jeong and J. Y. Lee, Dibenzothiophene derivatives as host materials for high efficiency in deep blue phosphorescent organic light emitting diodes, *J. Mater. Chem.*, 2011, **21**, 14604–14609.

57 X. Yao, H. Ma, X. Wang, H. Wang, Q. Wang, X. Zou, Z. Song, W. Jia, Y. Li, Y. Mao, M. Singh, W. Ye, J. Liang, Y. Zhang, Z. Liu, Y. He, J. Li, Z. Zhou, Z. Zhao, Y. Zhang, G. Niu, C. Yin, S. Zhang, H. Shi, W. Huang and Z. An, Ultralong organic phosphorescence from isolated molecules with repulsive interactions for multifunctional applications, *Nat. Commun.*, 2022, **13**, 4890.

58 H. Wu, W. Chi, Z. Chen, G. Liu, L. Gu, A. K. Bindra, G. Yang, X. Liu and Y. Zhao, Achieving Amorphous Ultralong Room Temperature Phosphorescence by Coassembling Planar Small Organic Molecules with Polyvinyl Alcohol, *Adv. Funct. Mater.*, 2019, **29**, 1807243.

59 Y. Zhou, W. Qin, C. Du, H. Gao, F. Zhu and G. Liang, Long-Lived Room-Temperature Phosphorescence for Visual and Quantitative Detection of Oxygen, *Angew. Chem., Int. Ed.*, 2019, **58**, 12102–12106.

60 Z. Liang, M. Wei, S. Zhang, W. Huang, N. Shi, A. Lv, H. Ma and Z. He, Activating Molecular Room-Temperature Phosphorescence by Manipulating Excited-State Energy Levels in Poly(vinyl alcohol) Matrix, *ACS Appl. Mater. Interfaces*, 2023, **15**, 35534–35542.

61 H. Ma, Q. Peng, Z. An, W. Huang and Z. Shuai, Efficient and Long-Lived Room-Temperature Organic Phosphorescence: Theoretical Descriptors for Molecular Designs, *J. Am. Chem. Soc.*, 2019, **141**, 1010–1015.

62 N. Aizawa, Y.-J. Pu, Y. Harabuchi, A. Nihonyanagi, R. Ibuka, H. Inuzuka, B. Dhara, Y. Koyama, K.-i. Nakayama, S. Maeda, F. Araoka and D. Miyajima, Delayed fluorescence from inverted singlet and triplet excited states, *Nature*, 2022, **609**, 502–506.

63 H. Noda, X.-K. Chen, H. Nakanotani, T. Hosokai, M. Miyajima, N. Notsuka, Y. Kashima, J.-L. Brédas and C. Adachi, Critical role of intermediate electronic states for spin-flip processes in charge-transfer-type organic molecules with multiple donors and acceptors, *Nat. Mater.*, 2019, **18**, 1084–1090.

64 A. L. Schleper, K. Goushi, C. Bannwarth, B. Haehnle, P. J. Welscher, C. Adachi and A. J. C. Kuehne, Hot exciplexes in U-shaped TADF molecules with emission from locally excited states, *Nat. Commun.*, 2021, **12**, 6179.

65 B. Li, J. Lou, H. Zhang, G. Li, X. He, Y. Huang, N. Zheng, Z. Wang, D. Ma and B. Z. Tang, “Exciton Recovery” Strategy in Hot Exciton Emitter toward High-Performance Non-Doped Deep-Blue and Host-Sensitized Organic Light-Emitting Diodes, *Adv. Funct. Mater.*, 2023, **33**, 2212876.

66 Y. Yang, F. Geng, Z. Jiang, Y. Liu, T. Guan, C. Qin, C. Zhuang and Y. Liu, Ultrafast dynamics of mCP and Br-mCP: Insights from transient absorption spectroscopy, *J. Lumin.*, 2025, **277**, 120940.

67 Y. Yang, Z. Jiang, Y. Liu, T. Guan, Q. Zhang, C. Qin, K. Jiang and Y. Liu, Transient Absorption Spectroscopy of a Carbazole-Based Room-Temperature Phosphorescent Molecule: Real-Time Monitoring of Singlet-Triplet Transitions, *J. Phys. Chem. Lett.*, 2022, **13**, 9381–9389.